Safe Charging for Wireless Power Transfer

Haipeng Dai, *Member, ACM*, Yunhuai Liu, Guihai Chen, Xiaobing Wu, Tian He, Alex X. Liu, and Huizhen Ma

***Abstract*— As battery-powered mobile devices become more popular and energy hungry, wireless power transfer technology, which allows the power to be transferred from a charger to ambient devices wirelessly, receives intensive interests. Existing schemes mainly focus on the power transfer efficiency but overlook the health impairments caused by RF exposure. In this paper, we study the safe charging problem (SCP) of scheduling power chargers so that more energy can be received while no location in the field has electromagnetic radiation (EMR) exceeding a given threshold R_t. We show that SCP is NP-hard and propose a solution, which provably outperforms the optimal solution to SCP with a relaxed EMR threshold $(1-\epsilon)R_t$. Testbed results based on 8 Powercast TX91501 chargers validate our results. Extensive simulation results show that the gap between our solution and the optimal one is only 6.7% when $\epsilon = 0.1$, while a naive greedy algorithm is 34.6% below our solution.**

***Index Terms*— Electromagnetic radiation, wireless power transfer, optimization.**

I. Introduction

AS BATTERY-POWERED mobile and portable devices become more popular and energy-hungry, energy conservation and scavenging schemes are increasingly important for the device usability. Among all such schemes, wireless power transfer technology [1] attracts intensive research and industry interest due to its convenience in applications. With this technology, energy can be transferred wirelessly from an energy storage to consuming devices such as RFIDs [2], sensors [3], cell phones [4], laptops [5], vehicles [6] and unmanned planes [7]. According to a recent report, the wireless power transfer market is expected to grow to US$17.04 billion in 2020 [8].

Manuscript received October 24, 2016; revised May 31, 2017; accepted August 18, 2017; approved by IEEE/ACM TRANSACTIONS on NETWORKING Editor C. Joo. Date of publication September 26, 2017; date of current version December 15, 2017. This work was supported in part by China 973 projects under Grant 2014CB340303, in part by the National Natural Science Foundation of China under Grant 61502229, Grant 61672353, Grant 61472252, Grant 61321491, Grant 61332018, Grant 61772046, Grant 61629302, Grant 61373130, Grant 61672276, and Grant 61472184, in part by the Natural Science Foundation of Jiangsu Province under Grant BK20141319, in part by the National Science Foundation under Grant CNS-1318563, Grant CNS-1524698, and Grant CNS-1421407, in part by IIP-1632051, and in part by the Jiangsu High-level Innovation and Entrepreneurship (Shuangchuang) Program. *(Corresponding authors: Yunhuai Liu; Guihai Chen; Tian He.)*

H. Dai, G. Chen, and H. Ma are with the State Key Laboratory for Novel Software Technology, Nanjing University, Nanjing 210023, China (e-mail: haipengdai@nju.edu.cn; gchen@nju.edu.cn; mg1533037@smail.nju.edu.cn).

Y. Liu is with Peking University, Beijing 100080, China (e-mail: yunhuai.liu@pku.edu.cn).

X. Wu is with the Wireless Research Centre, University of Canterbury, Christchurch 8041, New Zealand (e-mail: barry.wu@canterbury.ac.nz).

T. He is with the Computer Science and Engineering Department, University of Minnesota, Minneapolis, MN 55455 USA (e-mail: tianhe@cs.umn.edu).

A. X. Liu is with the State Key Laboratory for Novel Software Technology, Nanjing University, Nanjing 210023, China, and also with the Department of Computer Science, Michigan State University, East Lansing, MI 48824 USA (e-mail: alexliu@cse.msu.edu).

This paper has supplementary downloadable material available at http://ieeexplore.ieee.org., provided by the author.

Digital Object Identifier 10.1109/TNET.2017.2750323

In existing studies, researchers focused more on the energy charging efficiency and ubiquitousness, targeting at the minimal number of active chargers with more charging coverage (*e.g.*, [9]–[16]). In practice, however, this is far from enough. Besides the charging efficiency, a more critical issue is the safety of the electromagnetic radiation (EMR). Exposure to high EMR has been widely identified as a threat to human health. For example, Olteanu *et al.* [17] investigated the harmful effect of metallic implant heating resulted from EMR around, which may lead to impairment of issues. And it is reported that heating of tissue that exceeds 1 degree centigrade may interfere with behavioral and biological functions [18]. Gandhi *et al.* [19] found that children's heads absorb over two times of RF than adults, and absorption of the skull's bone marrow can be ten times greater than adults. Tissues of fetus, such as the central nervous system, seem especially vulnerable to temperature rises caused by high EMR in various time windows, particularly during organogenesis [20]. Changes on gene/protein expression by RF exposure are also investigated. Leszczynskis group performed a pilot study on volunteers and showed that mobile phone radiation might alter protein expression in human skin cells [21]. Nittby *et al.* [22] found that a large number of genes were altered at hippocampus and cortex using four exposed and four control animals. Though no actual experiments have been conducted concerning the potential harm to people, plenty of clinical studies such as [23] showed an increased risk of high EMR exposure for brain tumors. Besides, the link between RF exposure and mental diseases has also been confirmed. Experiments done on mice [24] showed that EMR causes transient and cumulative impairments in spatial and non-spatial memory. Concerns about adverse consequences of EMR exposure have resulted in the establishment of exposure limits. These limits are codified in Title 47 of the Code of Federal Regulations (CFR) in the United States and Hygienic Standard for Environmental Electromagnetic Waves GB9175-88 [25] in China, and also contained in standards published by the International Commission on Non-Ionizing Radiation Protection (ICNIRP) [26] in most of Europe. For instance, the maximum allowed power density for frequency $915\,MHz$, the commonly used frequency band for wireless power transfer, by CFR, GB9175-88 and ICNIRP are $610\,\mu W/cm^2$, $40\,\mu W/cm^2$ and $457.5\,\mu W/cm^2$, respectively. Consequently, a validated wireless charging scheme must comply with these regulations and guarantee the EMR safety in the field. No location should have the EMR value exceeding a certain EMR safety threshold.

With this practical and critical concern, in this paper, we propose and study the safe charging problem, attempting to strike the best tradeoff between the charging efficiency and EMR safety. Given a set of wireless power chargers and rechargeable devices, we are seeking the charger scheduling scheme so that the devices can obtain more power, while no location exceeds the EMR safety threshold.

Safe charging is a quite challenging problem which in general is NP-hard. The challenges are mainly due to the

fact that the EMR constraints are imposed on every point in the field, which inevitably results in an infinite number of constraints. In addition, as we will show in later sections, the objective function is a non-convex one, which prevents the classical optimization method to apply directly. To overcome these challenges, we design constraint conversion and reduction techniques and apply approximation approaches, which enable us to transfer the problem to a traditional multidimensional 0/1 knapsack problem [27] and a Fermat-Weber problem [28], *i.e.*, to find the optimal activation set of chargers maximizing the overall charging power under a limited number of constraints, and to find the point with the maximum EMR for a given active charger set. The constraints of the first problem are actually derived based on the outputs of the second problem.

The main contributions of this paper are as follows:

- To the best of our knowledge, this is the first work that considers charging efficiency under EMR safety concern. We formulate the problem as Safe Charging Problem (SCP), and show it is NP-hard.
- To deal with the problem, we design a series of novel techniques to transfer the problem to two traditional problems, namely a multidimensional 0/1 knapsack problem and a Fermat-Weber problem. The techniques include constraint conversion and reduction, bounded EMR function approximation, area discretization and expansion, and a tailored Fermat-Weber algorithm.
- We prove that for any given small number ϵ, our solution outperforms the optimal solution to SCP with a relaxed EMR threshold $(1-\epsilon)R_t$, where R_t is the original EMR threshold.
- To evaluate the performance of our algorithm, we build a testbed composed of 8 Powercast TX91501 chargers. Experimental results show that the maximal EMR in the field is $116.7\,\mu W/cm^2$, which is just below the safety threshold of $125\,\mu W/cm^2$. We also conduct comprehensive simulations and the gap between our solution and the optimal one is only 6.7% when $\epsilon = 0.1$, while a naive greedy algorithm is 34.6% below our solution.

The remainder of the paper is organized as follows. In Section II, we briefly review related work. In Section III, we give preliminaries and a formal definition of the SCP problem. We introduce a near optimal solution to SCP in Section IV based on the theoretical results of MEP computation in Section V. Section VI and Section VII present extensive simulations and testbed experiments to verify our theoretical results, and Section VIII concludes.

II. Related Work

There is a multitude of works dedicated to wireless power transfer technology, and we refer readers to [29]–[31] for comprehensive surveys. First, there are some wireless charging works regarding scenarios with stationary chargers that don't consider EMR safety. Recently, Intel developed the wireless identification and sensing platform (WISP) by integrating RFID tags with sensing and computing components. The RFID tags can be wirelessly charged by readers. Buettner *et al.* [9] explored this technology to recognize human activities in, and highlighted applications such as elderly care in [10]. In [11], Powercast developed a wireless power platform to work with wireless sensor network. Their objective was to help monitor temperature and humidity at a zoo without disrupting the animal exhibit. This company also offered a solution for data center environmental monitoring by constructing a network of chargers [12]. He *et al.* [13] studied the energy provisioning problem, *i.e.*, how to deploy chargers to provide sufficient energy to static/mobile devices in wireless rechargeable sensor networks. Zhang *et al.* [32] studied the problem of charger placement and power allocation where chargers can be placed at a given set of points and the aggregate power supply of chargers is bounded by a power budget. Their goal is to maximize the overall charging utility. Wicaksono *et al.* [14] considered the power interference when allocating frequency bands to adjacent stationary chargers. Katsidimas *et al.* [33] presented a more realistic model for power harvesting by capturing the fundamental properties of the superposition of energy fields for wireless power transfer, and studied how to maximize the total power in the system. Unlike previous literatures that adopt omnidirectional charging models, we proposed a directional charging model where both the charging coverage area for chargers and receiving area for devices can be modeled as sectors, and considered ominidirectional charging using directional chargers in [34], and the directional wireless charger placement problem in [35].

Second, there are related works taking EMR safety into consideration, but few of them consider scheduling issues for wireless chargers with adjustable power. In the conference version of this paper [36], we considered the charging utility maximization problem by first taking the EMR safety into consideration and assuming that chargers can only be in either on or off status. We further extended the safe charging problem to the scenario where the power of chargers can be continuously adjusted in [37], and proposed a distributed algorithm. Moreover, we studied the charger placement problem in [38] and fair charging problem in [39]. In [40], we for the first time investigated the charging task scheduling problem under the EMR safety constraint, and proposed both centralized and distributed algorithms with near optimal performance in terms of the aggregate charging energy and the total charging time. Nikoletseas *et al.* [41] proposed a scheme to optimize the useful energy transferred from chargers to nodes under several realistic constraints such as finite limited energy supplies of chargers and finite battery capacity of nodes.

III. Problem Statement

In this paper, we assume all the chargers and rechargeable devices are static and deployed in fixed, known locations. We consider a simplified charger scheduling model in which chargers can be only in either of the on/off status. More complicated deployment schemes (*e.g.*, mobile chargers) and scheduling models (*e.g.*, adjustable charger power) are left for future work. Ideally, the charging scheme should on one hand maximize the charging efficiency so that more charging energy can be harvested by the rechargeable devices, and on the other hand ensure the safety of the field by limiting the intensity of EMR at every position in the field. To achieve this goal, we will formulate the problem and propose our solutions in the remainder of this paper. In this section, we will first give the system and charging model, and then provide the formal problem statement.

A. System and Charging Model

Assume there is a set of n identical stationary wireless power chargers $S = \{s_1, s_2, \ldots, s_n\}$ deployed on a two-dimensional plane, and a set of m rechargeable devices $O = \{o_1, o_2, \ldots, o_m\}$ in the field too. The devices are capable

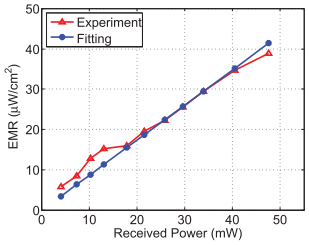

Fig. 1. EMR vs. received power. (a) Set of uniform cones. (b) Coordinates.

of harvesting the wireless power originated from chargers to maintain their normal working.

In general, both the wireless charging power and the EMR intensity are related to the energy field strength. The received power $P_r(d)$ by a device can be quantified by an empirical model [13], *i.e.*,

$$P_r(d) = \begin{cases} \dfrac{\alpha}{(d+\beta)^2}, & d \le D \\ 0, & d > D \end{cases} \tag{1}$$

where d is the distance from the charger to the receiver, and α and β are known constants determined by hardware of the charger and the receiver and the environment. Because of the hardware constraint, the energy field far away from the charger will be too small to be received by a node, and we use D to denote the farthest distance a charger can reach. In addition, we assume the wireless power from multiple chargers to a receiver is additive [13], and define the charging utility to be proportional to the charging power, namely

$$u(o_j) = c_1 \sum_{i=1}^{n} P_r(d(s_i, o_j)) \tag{2}$$

where $d(s_i, o_j)$ is the distance from the charger s_i to the device o_j, and c_1 is a predetermined constant.

Similarly, for all rechargeable devices, a charger s_i can provide charging utility as

$$u(s_i) = c_1 \sum_{j=1}^{m} P_r(d(s_i, o_j)). \tag{3}$$

For the intensity of EMR, we conduct field experiment studies and show the results in Fig. 1. Apparently, the EMR is nearly proportional to the received power, which can be modeled by $e(d) = c_2\ P_r(d)$ where d is the distance and c_2 is the constant to capture the linear relation. Assuming EMR is also additive, the accumulated EMR at a location p is thus

$$e(p) = \sum_{s_i \in S} e(d(s_i, p)) = c_2 \sum_{s_i \in S} P_r(d(s_i, p)). \tag{4}$$

Some symbols and notations used in this paper are summarized in Table I.

B. Problem Statement

To guarantee the EMR safety, we have to examine every point on the plane to ensure that no place will have the EMR exceeding the hard threshold of EMR safety, which we denote by R_t. Mathematically, we can express the decision problem as follows

$$\forall p \in \mathbb{R}^2, \quad c_2 \sum\nolimits_{s_i \in S} P_r(d(s_i, p)) \le R_t.$$

TABLE I
NOTATIONS

Symbol	Meaning
s_i, S	Charger i, charger set
o_j, O	Device j, device set
$P_r(d)$	Received power from distance d
D	Farthest distance a charger can reach
$d(s_i, o_j)$	Distance from charger s_i to device o_j
$d(s_i, p)$	Distance from charger s_i to point p
$u(o_j)$	Charging utility of device o_j
$u(s_i)$	Charging utility provided by charger s_i
$e(d)$, $e(p)$	EMR from distance d, EMR at point p
x_i	Binary indicator denotes whether charger s_i is active or not
R_t	Hard threshold of EMR safety
Γ	List of effective active charger sets

Let x_i be a binary indicator that denotes whether charger s_i is active or not. For an active charger set specified by x_i, the above inequality can be rewritten as follows

$$\forall p \in \mathbb{R}^2, \quad c_2 \sum\nolimits_{i=1}^{n} P_r(d(s_i, p)) x_i \le R_t.$$

This inequality actually serves as the constraint of our problem. Moreover, our optimization goal is to maximize the overall charging utility from all the chargers, namely, $\sum_{i=1}^{n} u(s_i) x_i$. The Safe Charging Problem (SCP) can thus be defined as follows

$$\begin{aligned} \textbf{(SCP)} \ \max_{x_i} \ & c_1 \sum\nolimits_{i=1}^{n} \Big(\sum\nolimits_{j=1}^{m} P_r(d(s_i, o_j))\Big) x_i \\ \textit{s.t.} \ & \forall p \in \mathbb{R}^2, \quad c_2 \sum\nolimits_{i=1}^{n} P_r(d(s_i, p)) x_i \le R_t \\ & x_i \in \{0, 1\} \quad (i = 1, 2, \ldots, n). \end{aligned} \tag{5}$$

In the above formulation, x_i is an optimization variable. We call a location $p \in \mathbb{R}^2$ is "safe" if the EMR intensity at this location is no more than the threshold R_t, *i.e.*, $c_2 \sum_{i=1}^{n} P_r(d(s_i, p)) x_i \le R_t$, and is "danger" if otherwise. We assume a single charger will never cause the SCP problem, which indicates that $\frac{\alpha}{\beta^2} \le R_t$, because otherwise no chargers are allowed to be switched on and SCP becomes trivial. Besides, it is clear that the above formulation of SCP does NOT require that the combined charging coverage area is connected (*i.e.*, there is no isolated charging area formed by a subset of chargers). Therefore, our proposed scheme can be applied to the cases where the combined charging coverage area is connected or not. Nevertheless, if the coverage area is disconnected, we can decompose SCP into a few subprograms which corresponds to different isolated charging areas, and address them separately and obtain the same or even better results with less computational cost.

To solve SCP, we are mainly facing the following challenges. First, the constraint in SCP is imposed on every point on the plane. In other words, there is indeed an infinite number of constraints, which makes the problem extremely difficult. Second, even if we can reduce the number of constraints to a limited number, we will show later that SCP is in the form of a multidimensional 0/1 knapsack problem, which is NP-hard.

Theorem 1: SCP is NP-hard.

Proof: We sketch the proof here due to space limitation. As the constraints of SCP are non-linear, SCP is thus a non-linear program. According to [42], non-linear programming problems are generally NP-hard. Therefore, SCP is NP-hard. □

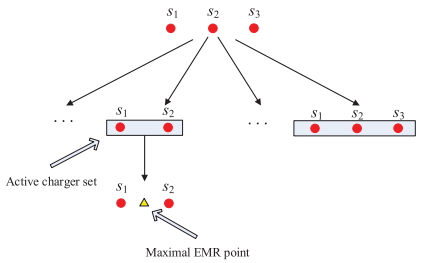

Fig. 2. An illustrative example of constraint conversion. For the set of active chargers s_1 and s_2, there will be a maximal EMR point (MEP) located between s_1 and s_2, and a corresponding constraint. Different active charger sets will have different MEPs.

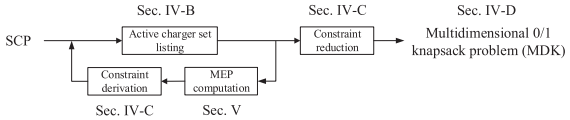

Fig. 3. SCP workflow.

In the remainder of this paper, we show how to solve SCP with a near optimal solution.

IV. A Near Optimal Solution

In this section, we introduce our solution to SCP and show that the algorithm has near optimal performance. We first depict the roadmap of our solution, and then present the techniques we applied individually in details.

A. Principles and Solution Workflow

As we mentioned before, the major challenge of SCP is that SCP has an infinite number of constraints when optimizing the objective function. To overcome this challenge, we propose two techniques, namely constraint conversion and constraint reduction, to reduce the number of constraints to a limited and tractable number. By this means, SCP will be reduced to a typical multidimensional 0/1 knapsack problem.

The constraint conversion is based on a simple observation. Given a set of active chargers, there will be one point having the maximal EMR intensity, which we call Maximal EMR Point (MEP) (if there is a set of points with the same maximal EMR intensity, we can arbitrarily pick one of them without affecting the correctness of our solution). When the MEP does not exceed R_t and is safe, other locations will be safe too. If the MEP is danger, the constraint is already violated. For the example in Fig. 2, suppose there are three chargers s_1, s_2, and s_3. Consider the active charger set of s_1 and s_2 (*i.e.*, s_3 is inactive). The MEP will be somewhere in between, say location p. For this case, we only need to check whether p exceeds R_t and derive a corresponding constraint. Note that different active charger sets will have different MEPs, and thus for SCP we shall check all the possible combinations of the active charger sets, compute the MEPs under the active chargers, and rewrite the constraints accordingly. With n chargers, there will be 2^n MEPs and 2^n constraints, which is sufficient. Nevertheless, concerning the practical reasons, we find that the number of effective constraints can be significantly reduced, which will be introduced in a later subsection.

Fig. 3 depicts the workflow of our solution. Given an instance of SCP, we first apply the constraint reduction to list all effective active charger sets (Section IV-B), compute the MEP under the charger set and derive the corresponding constraint (Section IV-C). Then, we employ constraint reduction approach to reduce the number of obtained constraints (Section IV-C). As such SCP is reformulated to a typical multidimensional 0/1 knapsack problem (MDK), we will give the approximation algorithm for MDK in Section IV-D. Since the computation of MEP is quite complex, we skip it in this section and describe it separately in Section V.

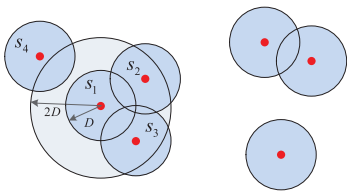

Fig. 4. Active charger set listing.

B. Active Charger Set Listing

In the active charger set listing, the input is n chargers and their locations, and the output is a list of active charger sets used to derive constraints. Intuitively, each possible charger set will have its MEP and each MEP will lead to a corresponding constraint. In the worst case, for n chargers, there will be 2^n active charger sets and thus 2^n constraints as well. This is, however, neither practical nor necessary for further processing.

As shown in Fig. 4, since every MEP must lie in the covered region of a certain charger, we only have to investigate the covered region for each charger. For example, for the disk region covered by s_1 with radius D, which is the farthest distance that a charger can reach in Eq. 1, an MEP within it can only be charged by chargers with distance less than D. In other words, only the chargers with distance to s_1 less than $2D$, *i.e.* s_2 and s_3, are able to reach the MEP. The number of these chargers is at most $\rho\pi\ (2D)^2$, where ρ is the charger deployment density. By enumerating all possible active charger sets for the covered region of each charger, we obtain in total $O(n2^{4\rho\pi D^2})$ constraints. We note that ρ can be interpreted as the maximum charger density when we analyze the time complexity and consider the worst case performance. If the density is relatively uniform across the network, which is implicitly assumed in our time complexity analysis, then ρ is a constant determined by the coverage radius of chargers D, the number of chargers n, and the field size. After all, we stress that the purpose of setting ρ is only for convenience of time complexity analysis for our algorithm.

C. Constraint Derivation, Reduction and MDK

For each possible active charger set, we can derive the constraint based on its MEP. In Section V, we will show how to compute an MEP based on a given active charger set. Here we use the results directly.

Let Γ denote the lightweight list of effective active charger sets we obtained in the last subsection, and $S \in \Gamma$ be an active charger set in Γ. Suppose the MEP of S is at the location p. The constraint associated with S is

$$c_2 \sum\nolimits_{s_i \in S} P_r(d(s_i, p))x_i \leq R_t. \tag{6}$$

The obtained constraints by this method can be reduced by removing the following two types of constraints: (i) trivial

Algorithm 1 Approximation Algorithm for SCP

INPUT A set of n chargers $s_i \in S, i = 1, \ldots, n$, and a set of m rechargeable devices $o_j \in O, j = 1, \ldots, m$
OUTPUT Binary indicator $x_i \in \{0, 1\}, i = 1, \ldots, n$
1: **for all** charger s_i **do**
2: Let A be the disk area centered at s_i with radius $2D$;
3: Identify all chargers within A;
4: **for all** active charger set S of chargers in A **do**
5: Compute MEP with error threshold $\epsilon/2$ based on the active charger set S;
6: Derive constraint based on the MEP using Eq. 6;
7: **end for**
8: **end for**
9: Conduct constraint reduction;
10: Reformulate SCP based on Eq. 7 and modify the EMR threshold R_t to $(1 - \epsilon/2)R_t$;
11: Use Algorithm 1 in [43] with error threshold $\epsilon/2$ to compute the solution $x_1, \ldots, x_n$ of the reformulated SCP.

constraints that can be always satisfied, which means its corresponding active charger set should never lead to an EMR exceeding R_t; (ii) redundant constraints that can be safely removed if at least one of the subsets of its corresponding active charger set leads to an EMR exceeding R_t. For example, if active charger set of s_1 and s_2 has already violated EMR safety, it is needless to include the constraint of its superset of s_1, s_2 and s_3.

With the reduced constraints set Γ, SCP is reformulated as

$$\textbf{(SCP)} \ \max_{x_i} \ c_1 \sum\nolimits_{i=1}^{n} (\sum\nolimits_{j=1}^{m} P_r(d(s_i, o_j)))x_i$$
$$s.t. \ \forall S \in \Gamma, \quad c_2 \sum\nolimits_{s_i \in S} P_r(d(s_i, p))x_i \le R_t$$
$$x_i \in \{0, 1\} \quad (i = 1, 2, \ldots, n). \tag{7}$$

This is a typical MDK problem [27]. When the number of constraint $|\Gamma| \ge 2$, there does not exist an FPTAS unless $P = NP$ [27]. We here apply an algorithm proposed in [43] to obtain an approximation solution.

D. Algorithm Description and Results

Algorithm 1 presents the pseudo-code of the approximation algorithm. The input of our algorithm is the set of chargers, devices and their locations. The output of the algorithm is the binary indicator x_i to control whether a charger should be active or not. The following theorem describes the performance of Algorithm 1.

Theorem 2: The time complexity of Algorithm 1 is $O(n^4(\epsilon^{-2}+\epsilon^{-3/2}n)+n(\frac{n}{\epsilon})^{|\Gamma|})$. *The output of Algorithm 1 is a feasible solution of SCP, and outperforms the optimal solution to SCP with a smaller EMR threshold* $(1 - \epsilon)R_t$.

Proof: By Theorem 14, the overall time complexity for computing one single constraint in SCP is $O(\epsilon^{-2}n^3 + \epsilon^{-3/2}n^4)$. Moreover, according to analysis in Section IV-B, we have to compute at most $O(n2^{4\rho\pi D^2}) = O(n)$ constraints. The whole time complexity for computing constraints is thus $O(n^4(\epsilon^{-2} + \epsilon^{-3/2}n))$. Besides, by [43, Th. 3.2], the time complexity to compute the solution at Step 11 in Algorithm 1 is $O(n(\frac{n}{\epsilon})^{|\Gamma|}))$. To sum up, the overall time complexity of Algorithm 1 is $O(n^4(\epsilon^{-2} + \epsilon^{-3/2}n) + n(\frac{n}{\epsilon})^{|\Gamma|})$.

Next we analyze the performance of Algorithm 1. By Theorem 14, the output $p^{\#}$ of the MEP approximation algorithm applied at Step 5 of Algorithm 1 satisfies

$$(1 - \frac{\epsilon}{2})c_2 \sum\nolimits_{s_i \in S} P_r(d(s_i, p))x_i \le c_2 \sum\nolimits_{s_i \in S} P_r(d(s_i, p^{\#}))x_i. \tag{8}$$

We then let

$$c_2 \sum\nolimits_{s_i \in S} P_r(d(s_i, p^{\#}))x_i = (1 - \epsilon_i)c_2 \sum\nolimits_{s_i \in S} P_r(d(s_i, p))x_i \tag{9}$$

where ϵ_i is an unknown constant and is subject to $0 \le \epsilon_i \le \epsilon/2$. Then SCP can be reformulated as follows

$$\textbf{(SCP)} \ \max_{x_i} \ c_1 \sum\nolimits_{i=1}^{n} (\sum\nolimits_{j=1}^{m} P_r(d(s_i, o_j)))x_i$$
$$s.t. \ \forall S \in \Gamma, \quad c_2 \sum\nolimits_{s_i \in S} P_r(d(s_i, p^{\#}))x_i \le \frac{1}{1-\epsilon_i} R_t$$
$$x_i \in \{0, 1\} \quad (i = 1, 2, \ldots, n).$$

As ϵ_i is unknown, we turn to seek the solution to a reformulated problem at Step 10 of Algorithm 1:

$$\textbf{(SCP-R)} \ \max_{x_i} \ c_1 \sum\nolimits_{i=1}^{n} (\sum\nolimits_{j=1}^{m} P_r(d(s_i, o_j)))x_i$$
$$s.t. \ \forall S \in \Gamma, \quad c_2 \sum\nolimits_{s_i \in S} P_r(d(s_i, p^{\#}))x_i \le (1 - \frac{\epsilon}{2})R_t$$
$$x_i \in \{0, 1\} \quad (i = 1, 2, \ldots, n).$$

Because $\frac{1}{1-\epsilon_i} R_t \ge (1 - \frac{\epsilon}{2})R_t$, any feasible solution to SCP-R is also feasible to SCP. Furthermore, because $(1 - \epsilon/2) \le \frac{1-\epsilon/2}{1-\epsilon_i} \le 1$, the optimal solution to SCP-R should outperform the optimal solution to SCP with a smaller EMR threshold $(1 - \epsilon/2)R_t$. As there is no optimal solution to SCP-R, we use a near optimal algorithm proposed in [43]. Nevertheless, our approximation solution is still feasible to SCP-R, and thus feasible to SCP. More importantly, though additional error may be introduced, the applied algorithm with error threshold $\epsilon/2$ at Step 11 of Algorithm 1 gurantees to obtain a solution outperforming the optimal solution to SCP-R with the constant in the right side of each linear constraint being reduced by a factor $(1 - \epsilon/2)$. Consequently, the output of Algorithm 1 should outperform the optimal solution to SCP with a smaller EMR threshold $(1 - \epsilon/2) * (1 - \epsilon/2)R_t$, and thus outperforms the optimal solution to SCP with threshold $(1 - \epsilon)R_t$. This completes the proof. □

V. MEP Computation

In this section, we compute MEP for a given active charger set. This is a major but difficult problem when solving SCP. The main challenges are as follows. First, the objective function $e(p)$ in Eq. 4 is non-convex, and thus there is no standard solution to be global optimal. Second, the search space of MEP is continuous, but the output is a single point. In what follows, we first give the main results, and then present our approximation algorithm.

A. Algorithm Overview

The key idea of MEP computation is to approximate the non-convex EMR function $e(p)$ by a set of convex functions so that the problem can be transformed into the traditional

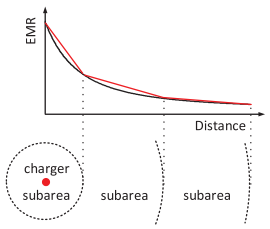

Fig. 5. Piecewise linear approximation.

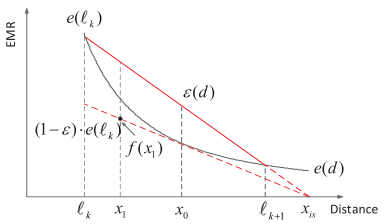

Fig. 6. Illustration of proof for Theorem 6.

Fermat-Weber problem [28]. The workflow of our algorithm is as follows. We first use a piecewise linear function $\varepsilon(d)$ to approximate $e(d)$ (Section V-B), and thereby, the covered area of a charger is partitioned to many subareas. Subareas of different chargers will overlap to further partition the area, and each partitioned subarea has a convex objective function (Section V-C). Nevertheless, shapes of some subareas may become non-convex, which is difficult to be tackled. We thus expand the subareas to convex ones with performance guarantee in the third step (Section V-D). By these means, the MEP computation problem can be transformed into the traditional Fermat-Weber problem with norm constraints (Section V-E). The MEP of the whole area is then among these subarea MEPs and easy to find.

For better understanding these procedures, we present the formal definition of the Fermat-Weber problem with norm constraints. Then, we present the detailed steps of the MEP computation algorithm in the following subsections.

Definition 3 (Fermat-Weber Problem With Norm Constraints (FWNC)): Let $S = \{s_1, s_2, \ldots, s_n\}$ be a set of points in $\mathbb{R}^2$, the Weber-Fermat problem is a facility problem that aims to find the point p such that

$$\min_{p} \sum_{i \in n} w_i d(s_i, p) \quad \text{s.t. } d(s_i, p) \le C_i, \quad i = 1, 2, \ldots, n. \tag{10}$$

where w_i and C_i are constants.

B. Piecewise Linear Approximation of $e(d)$

Essentially, we use multiple piecewise linear segments $\varepsilon(d)$ to approximate the EMR function $e(d)$ (recall $e(d) = c_2\ P_r(d)$), and meanwhile, try to bound the approximation error $\varepsilon(d) - e(d)$ and the computational overhead.

The basic idea of the approximation $\varepsilon(d)$ is illustrated in Fig. 5. Let the vector $L = \{\ell_0, \ell_1, \ldots, \ell_K\}$ be the end points of K linear segments in an increasing sequence. The parameter K is the number of segments that controls the approximation error. In the example of Fig. 5, K is equal to 3. Basically, a larger K will result in a smaller approximation error but introduce more computation overhead.

Definition 4: Setting $\ell_0 = 0$ and $\ell_K = D$, the piecewise approximation function $\varepsilon(d)$ can be defined as

$$\varepsilon(d) = \begin{cases} -w_k d + \phi_k, & \ell_{k-1} \le d \le \ell_k \quad (k = 1, \ldots, K) \\ 0, & d > D \end{cases} \tag{11}$$

where $\phi_k = \frac{e(\ell_k)\ell_{k+1} - e(\ell_{k+1})\ell_k}{\ell_{k+1} - \ell_k}\ (\phi_k > 0)$ and $w_k = -\frac{e(\ell_{k+1}) - e(\ell_k)}{\ell_{k+1} - \ell_k}\ (w_k > 0)$ when $k \le K$; otherwise $\phi_k = w_k = 0$.

Definition 5: To bound the approximation error, we set ℓ_{k+1} (if the obtained $\ell_{k+1} \ge D$, set $K = k + 1$, $\ell_{k+1} = D$) sequentially based on ℓ_k ($\ell_0 = 0$) in Eq. 11 as

$$\ell_{k+1} = \frac{1}{4}(3x_0 - 2\ell_k + \beta + \sqrt{(3x_0 - 2\ell_k + \beta)(3x_0 + 6\ell_k + 9\beta)}) - \beta \tag{12}$$

where β is a constant in Eq. 1, and x_0 is one of the roots to the following cubic equation

$$\frac{1 - \epsilon}{(\ell_k + \beta)^2}(x_0 + \beta)^3 - 3x_0 + 2\ell_k - \beta = 0$$

that satisfies $x_0 > \ell_k$.

By these definitions, we have

Theorem 6: Setting ℓ_{k+1} by Eq. 12, we have the approximation errors as $e(d) \le \varepsilon(d) \le \frac{e(d)}{1-\epsilon}$.

Proof: We prove the theorem by showing that given the above approximation error requirement, the maximum value of ℓ_{k+1} should be subject to Eq. 12.

As shown in Fig. 6, suppose the extended line of the approximation line segment intersects the horizontal axis at point x_{is}. Suppose there is a line passing through x_{is} and being tangent to the curve $e(d)$ at point x_0, and its corresponding function is $f(d)$. We claim that the error function $\frac{\varepsilon(d) - e(d)}{\varepsilon(d)}$ for $\ell_k \le d \le \ell_{k+1}$ exactly maximizes at point x_0, and is equal to ϵ. To see this, suppose there is another point x_1 ($\ell_k \le x_1 \le \ell_{k+1}, x_1 \ne x_0$), and its corresponding value on the line $f(d)$ is $f(x_1)$, then it is clear that

$$\frac{\varepsilon(x_1) - e(x_1)}{\varepsilon(x_1)} < \frac{\varepsilon(x_1) - f(x_1)}{\varepsilon(x_1)} = \frac{\varepsilon(x_0) - e(x_0)}{\varepsilon(x_0)}. \tag{13}$$

Note that the last equation is a straightforward geometric observation.

As $f(d)$ is tangent to $e(d)$ at point x_0, $f(d)$ is given by $f(d) = \frac{c_2\alpha}{(x_0+\beta)^2} - \frac{2c_2\alpha}{(x_0+\beta)^3}(d - x_0)$. Further, as the line $f(d)$ passes through point $(\ell_k, (1-\epsilon)\cdot e(\ell_k))$, we have $f(\ell_k) = (1-\epsilon)\cdot e(\ell_k)$, and therefore,

$$\frac{1 - \epsilon}{(\ell_k + \beta)^2}(x_0 + \beta)^3 - 3x_0 + 2\ell_k - \beta = 0.$$

Though there are three roots to this cubic equation, we can pick out the proper root x_0 since $x_0 > \ell_k$.

Next, since the line $f(d)$ passes through point x_{is}, which means $f(x_{is}) = 0$, and thus $x_{is} = \frac{3}{2}x_0 + \frac{1}{2}\beta$. Moreover, as the three points $(\ell_k, e(\ell_k))$, $((\ell_{k+1}, e(\ell_{k+1})))$ and $(x_{is}, 0)$ are collinear, we have $e(\ell_{k+1}) = e(\ell_k) - \frac{\ell_{k+1} - \ell_k}{x_{is} - \ell_k}e(\ell_k)$, and therefore

$$2(\ell_{k+1} + \beta)^2 - (2x_0 - 2\ell_k + \beta)(\ell_k + \ell_{k+1} + 2\beta) = 0. \tag{14}$$

Solving this quadratic equation we obtain

$$\ell_{k+1} = \frac{1}{4}(3x_0 - 2\ell_k + \beta + \sqrt{(3x_0 - 2\ell_k + \beta)(3x_0 + 6\ell_k + 9\beta)}) - \beta, \tag{15}$$

which is exactly the value defined in Eq. 12. □

Theorem 7: If $\epsilon \to 0$, the number of linear segments K is subject to

$$\frac{\sqrt{3}}{4}(1-\frac{1}{(1+D/\beta)^2})\epsilon^{-1/2} < K < \frac{\sqrt{3}}{4}((1+D/\beta)^2-1)\epsilon^{-1/2}. \tag{16}$$

In other words, we have $K = \Theta(\epsilon^{-1/2})$.

Proof: Given $\epsilon \to 0$, $x_0 - \ell_k$ (see Definition 5) also approaches 0 according to the proof for Theorem 6. By using two order approximation of Taylor expansion, the cubic equation of x_0 can be approximated as

$$\begin{aligned}
&\frac{1-\epsilon}{(\ell_k+\beta)^2}(x_0+\beta)^3 - 3x_0 + 2\ell_k - \beta \\
&= \frac{1-\epsilon}{(\ell_k+\beta)^2}(1+\frac{x_0-\ell_k}{\ell_k+\beta})^3 \cdot (\ell_k+\beta)^3 - 3x_0 + 2\ell_k - \beta \\
&\approx (1-\epsilon)(1+3\frac{x_0-\ell_k}{\ell_k+\beta} + 3(\frac{x_0-\ell_k}{\ell_k+\beta})^2)\cdot(\ell_k+\beta) - 3x_0 \\
&\quad + 2\ell_k - \beta \\
&\approx 3\frac{(x_0-\ell_k)^2}{\ell_k+\beta} - \epsilon(\ell_k+\beta) \\
&= 0.
\end{aligned}$$

Hence, we have $x_0 \approx \ell_k + \frac{\sqrt{3}}{3}(\ell_k+\beta)\epsilon^{1/2}$, and,

$$\begin{aligned}
&\ell_{k+1} \\
&= \frac{1}{4}(3x_0 - 2\ell_k + \beta + \sqrt{(3x_0-2\ell_k+\beta)(3x_0+6\ell_k+9\beta)}) \\
&\quad - \beta \\
&= \frac{1}{4}(3x_0 - 2\ell_k + \beta + 3\sqrt{(1+3\frac{x_0-\ell_k}{\ell_k+\beta})(1+\frac{1}{3}\frac{x_0-\ell_k}{\ell_k+\beta})} \\
&\quad \cdot(\ell_k+\beta)) - \beta \\
&\approx \frac{1}{4}(3x_0 - 2\ell_k + \beta + 3(\ell_k+\beta)(1+\frac{5}{3}\frac{x_0-\ell_k}{\ell_k+\beta})) - \beta \\
&= 2x_0 - \ell_k \\
&\approx \ell_k + \frac{2\sqrt{3}}{3}(\ell_k+\beta)\epsilon^{1/2}.
\end{aligned}$$

Therefore, the length of projection of the linear segment at the horizontal axis is $\Delta x = \ell_{k+1} - \ell_k = \frac{2\sqrt{3}}{3}(\ell_k+\beta)\epsilon^{1/2}$. Its minimum value $\Delta x_{min} = \frac{2\sqrt{3}}{3}\beta\epsilon^{1/2}$ is achieved at $\ell_k = 0$, and the maximum value $\Delta x_{max} = \frac{2\sqrt{3}}{3}(\beta+D)\epsilon^{1/2}$ is achieved at $\ell_k \approx D$, as Fig. 7 shows. Accordingly, the length of projection of the linear segment at the vertical axis is

$$\Delta y \approx \Delta x \cdot e'(\ell_k) = \frac{4\sqrt{3}c_2\alpha}{3(\ell_k+\beta)^2}\epsilon^{1/2}. \tag{17}$$

Likewise, the minimum and maximum values of Δy are $\Delta y_{min} = \frac{4\sqrt{3}c_2\alpha}{3(D+\beta)^2}\epsilon^{1/2}$ and $\Delta y_{max} = \frac{4\sqrt{3}c_2\alpha}{3\beta^2}\epsilon^{1/2}$, respectively. Since the whole length of vertical projection of curve $e(d)$ is $e(0) - e(D)$, we can bound the number of linear segments K based on Δy_{min} and Δy_{max}, namely

$$\frac{e(0)-e(D)}{\Delta y_{max}} < K < \frac{e(0)-e(D)}{\Delta y_{min}}, \tag{18}$$

that is,

$$\begin{aligned}
\frac{\sqrt{3}}{4}(1-\frac{1}{(1+D/\beta)^2})\epsilon^{-1/2} &< K \\
&< \frac{\sqrt{3}}{4}((1+D/\beta)^2-1)\epsilon^{-1/2}.
\end{aligned} \tag{19}$$

Thus, we have $K = \Theta(\epsilon^{-1/2})$. This completes the proof. □

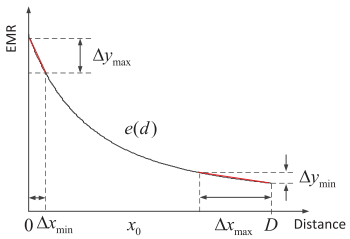

Fig. 7. Illustration of proof for Theorem 7.

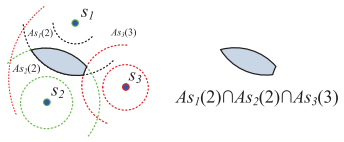

Fig. 8. Charging area discretization.

C. Discretizing Solution Space

By using piecewise linear segments $\varepsilon(d)$ to approximate $e(d)$, the covered area of a charger s, denoted as A_s, is partitioned to K concentric subareas denoted as $A_s(k), k = 1, \ldots, K$. Given the active charger set S, there will be at most $K|S|$ concentric subareas which may overlap with each other. According to the classical results in [44], $|S|$ chargers will partition the whole plane to at most Z subarea faces where

$$Z \le (K|S|)^2 - K|S| + 2 \le K^2|S|^2.$$

An illustration of such subarea faces with three chargers is depicted in Fig. 8. Note that we do not consider the area not covered by any chargers as obviously there has no EMR and MEP cannot be there.

By such partition, MEP for a given active charger set becomes to find MEP from each subarea face, and among these MEPs to find the one with the largest EMR. As the second step is straightforward, we here focus on the first step. Denote a subarea face overlapped by several chargers as $\mathcal{F}(\kappa) = \cap_{s_i \in S} A_{s_i}(k_i)$ where $\kappa = (k_1, k_2, ...k_{|S|})$ is a vector indicating the index of concentric subarea that shape the face. In Fig.8, the face is shaped by s_1's second subarea, s_2's second subarea, and s_3's third subarea, and thus it can be expressed as $\mathcal{F}(\kappa) = A_{s_1}(2) \cap A_{s_2}(2) \cap A_{s_3}(3)$ where $\kappa = \{2,2,3\}$. The accumulated EMR approximation for a location p in $\mathcal{F}(\kappa)$ is

$$\varepsilon(p) = \sum\nolimits_{s_i \in S}(-w_{k_i} d(s_i,p) + \phi_{k_i}), \quad p \in \mathcal{F}(\kappa). \tag{20}$$

Note w_{k_i} and ϕ_{k_i} defined in Eq. 11 are both constants within the concentric subarea $A_{s_i}(k_i)$. Therefore, maximizing $\varepsilon(p)$ is equivalent to minimizing $\sum_{s_i \in S} w_{k_i} d(s_i,p)$. Thus, MEP of an active charger set can be reformulated as

$$\max_{\forall \mathcal{F}(\kappa)} \{\varepsilon(p) | p = \min_{p \in \mathcal{F}(\kappa)} \sum_{s_i \in S} w_{k_i} d(s_i,p)\}. \tag{21}$$

D. Area Expansion

In the last subsection, MEP is reformulated with a convex objective function $\sum_{s_i \in S} w_{k_i} d(s_i,p)$. However, the subarea face $\cap_{s_i \in S} A_{s_i}(k_i)$ may become non-convex (see the example in Fig. 8), which makes traditional optimization methods infeasible. We deal with this issue in this subsection. We first propose an area expansion technique to transform non-convex areas to convex ones, and then prove its performance.

Fig. 9. Area expansion.

Definition 8: Denoting by $\Omega_{s_i}(k_i)$ the minimal enclosing disk of $A_{s_i}(k_i)$, $\Omega_{s_i}(k_i)$ is indeed the union of all concentric subareas no more than k_i, *i.e.*, $\Omega_{s_i}(k_i) = \cup_{k\le k_i} A_{s_i}(k)$. Then the expanded area $\Lambda(\kappa)$ for a subarea face $\mathcal{F}(\kappa)$ is defined as

$$\Lambda(\kappa) = \cap_{s_i\in S}\Omega_{s_i}(k_i) = \cap_{s_i\in S}(\cup_{k\le k_i} A_{s_i}(k)) \tag{22}$$

where $\kappa = (k_1, \ldots, k_{|S|})$.

Fig. 9 illustrates an example of area expansion based on the example in Fig. 8. After area expansion, the solution to MEP will not change, as the following theorem indicates.

Theorem 9: Suppose p^* and $\overline{p}^*$ are optimal solutions to the reformulated MEP defined in Eq. 21 before and after area expansion for each subarea, then $\varepsilon(p^*) = \varepsilon(\overline{p}^*)$.

Proof: The key idea of our proof is to prove $\varepsilon(p^*) \ge \varepsilon(\overline{p}^*)$ and $\varepsilon(p^*) \le \varepsilon(\overline{p}^*)$, then we have $\varepsilon(p^*) = \varepsilon(\overline{p}^*)$.

First of all, as the subarea $\mathcal{F}(\kappa)$ is expanded to $\Lambda(\kappa)$ (mathematically, we have $\mathcal{F}(\kappa) = \cap_{s_i\in S} A_{s_i}(k_i) \subseteq \cap_{s_i\in S}(\cup_{k\le k_i} A_{s_i}(k)) = \Lambda(\kappa)$), we accordingly extend the domain of definition of the original aggregate EMR computation function in $\mathcal{F}(\kappa)$ to $\Lambda(\kappa)$, and use $\varepsilon^{ext}(p)$ to denote the new function, *i.e.*,

$$\varepsilon^{ext}(p) = \sum\nolimits_{s_i\in S}(-w_{k_i} d(s_i, p) + \phi_{k_i}), p \in \Lambda(\kappa). \tag{23}$$

Note that $\varepsilon^{ext}(p) = \varepsilon(p)$ for $p \in \mathcal{F}(\kappa)$. We thus have $\max_{p\in\Lambda(\kappa)} \varepsilon^{ext}(p) \ge \max_{p\in\mathcal{F}(\kappa)} \varepsilon(p)$, and then,

$$\varepsilon^{ext}(\overline{p}^*) = \max_{\kappa\in\boldsymbol{\kappa}} \max_{p\in\Lambda(\kappa)} \varepsilon^{ext}(p) \ge \max_{\kappa\in\boldsymbol{\kappa}} \max_{p\in\mathcal{F}(\kappa)} \varepsilon(p) = \varepsilon(p^*). \tag{24}$$

Note that $\boldsymbol{\kappa}$ is the set of all vectors κ, and $|\boldsymbol{\kappa}| = Z$ where Z is the number of subarea faces.

We proceed to show that $\varepsilon(p^*) \le \varepsilon(\overline{p}^*)$. As the union of all expansion areas is exactly the area on the 2D plane that is covered by at least one charger, which is in turn formed by all original partitioned subarea faces. Thus, we have $\cup_{\kappa\in\boldsymbol{\kappa}}\Lambda(\kappa) = \cup_{\kappa\in\boldsymbol{\kappa}}\mathcal{F}(\kappa)$. Consequently, $\Lambda(\kappa)$ can be rewritten as $\Lambda(\kappa) = (\cup_{\kappa'\in\boldsymbol{\kappa}}\Lambda(\kappa')) \cap \Lambda(\kappa) = (\cup_{\kappa'\in\boldsymbol{\kappa}}\mathcal{F}(\kappa')) \cap \Lambda(\kappa) = \cup_{\kappa'\in\boldsymbol{\kappa}}(\mathcal{F}(\kappa') \cap \Lambda(\kappa))$ where $\kappa' = (k'_1, \ldots, k'_{|S|})$.

Next, we attempt to examine the EMR for each charger s_i in region $\mathcal{F}(\kappa') \cap \Lambda(\kappa)$, *i.e.*, the overlapping area of $\mathcal{F}(\kappa')$ and $\Lambda(\kappa)$. Suppose $\mathcal{F}(\kappa') \cap \Lambda(\kappa) \ne \emptyset$, otherwise the case is trivial. First, we have

$$\begin{aligned}\mathcal{F}(\kappa') \cap \Lambda(\kappa) &= (\cap_{s_i\in S} A_{s_i}(k'_i)) \cap (\cap_{s_i\in S}(\cup_{k\le k_i} A_{s_i}(k))) \\ &= \cap_{s_i\in S}(A_{s_i}(k'_i) \cap \cup_{k\le k_i} A_{s_i}(k)) \ne \emptyset,\end{aligned}$$

which indicates that $A_{s_i}(k'_i) \cap \cup_{k\le k_i} A_{s_i}(k) \ne \emptyset$. This result implies $k_i \ge k'_i$, and therefore subarea face $F(\kappa')$ must lie in the same concentric ring or an inner one compared with $F(\kappa)$ w.r.t. charger s_i. Hence, the EMR originated from charger s_i for any point $p \in \mathcal{F}(\kappa') \cap \Lambda(\kappa)$ is $-w_{k'_i} d(s_i, p) + \phi_{k'_i}$, $p \in \mathcal{F}(\kappa')$, while that provided by the extended function from region $\mathcal{F}(\kappa')$ to $\Lambda(\kappa)$ is $-w_{k_i} d(s_i, p) + \phi_{k_i}$, $p \in \Lambda(\kappa)$.

As $\varepsilon(d)$ is a monotonic decreasing and convex function and $k_i \ge k'_i$, we claim that $-w_{k'_i} d(s_i, p) + \phi_{k'_i} \ge -w_{k_i} d(s_i, p) + \phi_{k_i}$, $p \in \mathcal{F}(\kappa') \cap \Lambda(\kappa)$. We use Fig. 10 to illustrate this claim. Since $k_i \ge k'_i$, if we extend the domain of definition of the linear function in the k_i-th subarea to the k'_i-th subarea.

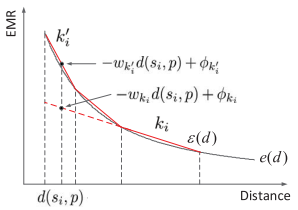

Fig. 10. Illustration of proof for Theorem 9.

For the same distance $d(s_i, p)$, the value of the extended function must be smaller than that of the function in the k'_i-th subarea.

Therefore, we have $\varepsilon^{ext}(p) = \sum_{s_i\in S}(-w_{k_i} d(s_i, p) + \phi_{k_i}) \le \sum_{s_i\in S}(-w_{k'_i} d(s_i, p) + \phi_{k'_i}) = \varepsilon(p)$ for $p \in \mathcal{F}(\kappa') \cap \Lambda(\kappa)$. Note that the sufficient condition for $\varepsilon^{ext}(p) = \varepsilon(p)$ is $\kappa = \kappa'$. Consequently, we have

$$\begin{aligned}\max_{p\in\Lambda(\kappa)} \varepsilon^{ext}(p) &= \max_{p\in\cup_{\kappa'\in\boldsymbol{\kappa}}(\mathcal{F}(\kappa')\cap\Lambda(\kappa))} \varepsilon^{ext}(p) \\ &= \max_{\kappa'\in\boldsymbol{\kappa}} \max_{p\in\mathcal{F}(\kappa')\cap\Lambda(\kappa)} \varepsilon^{ext}(p) \\ &\le \max_{\kappa'\in\boldsymbol{\kappa}} \max_{p\in\mathcal{F}(\kappa')\cap\Lambda(\kappa)} \varepsilon(p) \\ &\le \max_{\kappa'\in\boldsymbol{\kappa}} \max_{p\in\mathcal{F}(\kappa')} \varepsilon(p) \\ &= \varepsilon(p^*).\end{aligned} \tag{25}$$

Since κ is an arbitrary vector in $\boldsymbol{\kappa}$, it follows that

$$\varepsilon^{ext}(\overline{p}^*) = \max_{\kappa\in\boldsymbol{\kappa}} \max_{p\in\Lambda(\kappa)} \varepsilon^{ext}(p) \le \varepsilon(p^*). \tag{26}$$

Combining Inequality 24 with Inequality 26, we obtain $\varepsilon(p^*) = \varepsilon^{ext}(\overline{p}^*)$. Furthermore, we claim that $\varepsilon(\overline{p}^*) = \varepsilon^{ext}(\overline{p}^*)$. If not, we must have $\varepsilon(\overline{p}^*) > \varepsilon^{ext}(\overline{p}^*)$. We thus choose the extended function in subarea face κ', say $\varepsilon^{ext'}(p)$, which satisfies $\varepsilon^{ext'}(\overline{p}^*) = \varepsilon(\overline{p}^*) > \varepsilon^{ext}(\overline{p}^*)$. A contradiction arises, then we have $\varepsilon(p^*) = \varepsilon(\overline{p}^*)$. □

With all above, we reformulate MEP in each subarea as

$$\begin{aligned}&\min \sum_{s_i\in S} w_{k_i} d(s_i, p) \\ &s.t.\ d(s_i, p) \le \ell_{k_i}, \quad i = 1, 2, \ldots, |S|.\end{aligned} \tag{27}$$

Note that the above constraints stem from the definition of expanded area $\Lambda(\kappa)$. In the next subsection, we will show how to solve it by a modified Fermat-Weber problem algorithm.

E. Fermat-Weber Problem With Norm Constraints

Comparing MEP defined in Eq. 27 and the Fermat-Weber problem with norm constraints (FWNC) defined in Eq. 10, we find that they are exactly the same. The (weighted) Fermat-Weber problem, also known as the geometric median problem, is to find a point in $\mathbb{R}^n$ that minimizes the weighted sum of Euclidean distance from n given points [45]. It is also classified as a special version of the traditional facility problem [46]. Though the Fermat-Weber problem appears rather simple, so far no exact solution to the problem is known, even in the real RAM model of computation [47]. More discouraging, it has been proved even for 5 points, the coordinates of the optimal solution may not be presentable even if we allow radicals, and it is also impossible to construct the optimal solution by means of ruler and compass [48]. Motivated by this observation, [49] dedicated to compute an approximate solution using ellipsoid method, such that its

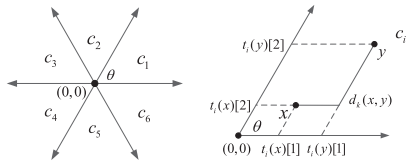

(a) (b)

Fig. 11. Illustration of skew coordinates. (a) Set of uniform cones. (b) Coordinates.

weighted sum is at most a $(1+\epsilon)$-factor larger than the cost of the optimal solution. A more efficient approximation algorithm achieving the same result was reported in [47]. To the best of our knowledge, [49] and [47] are two main approximation algorithms to the Fermat-Weber problem until now.

FWNC is a traditional problem that has been studied before [28]. There is, however, no effective solution for the problem. For instance, [28] presents optimal solutions to several special cases of FWNC, which cannot be applied to address our considered problem in this paper. Therefore, we tailor the approximation algorithm to unweighted Fermat-Weber problem constrained to a polyhedron in [47] to our case. Unlike the algorithm in [47] simply uses a binary search to find the optimal solution on the line segments of boundaries, our algorithm searches all the boundary arcs and adopts Lagrange multiplier method to optimize the objective function. Essentially, our algorithm is a fully polynomial time approximation scheme (FPTAS). We first introduce the following two key techniques extended from the techniques used in [47]. We make necessary adjustments and novel theoretical analysis for our case.

1) Coordinate System Transformation: The first technique is to transform 2D rectangular coordinates to a series of skew coordinates such that the distance for any query point q to the chargers can be approximated. We build a skew coordinate system formed by a set of uniform cones $C = \{c_1, c_2, \ldots, c_k\}$ that are defined by directions $\{0, 2\pi/k, 4\pi/k, \ldots, 2\pi(k-1)/k\}$. Fig. 11(a) shows an example where the number of cones, k, is set to 6, and therefore the angle of each cone is $\theta = \pi/3$. Furthermore, as shown in 11(b), we use vector $t_x(x)$ to denote the coordinates of point x in cone c_i, and notation $d_k(x, y)$ to denote the distance between any pair of points x and y. Denote by $||x||$ the sum $\sum_{j=1}^{2} x[j]$ for vector x, $d_k(x, y)$ can be expressed as $d_k(x, y) = ||t_i(y)|| - ||t_i(x)||$. We use $d_k(x, y)$ as the approximation for distance between any pair of points x and y, whose accuracy is bounded by the following lemma.

Lemma 10: For any pair of points $x, y \in \mathbb{R}^2$, $d(x, y) \leq d_k(x, y) \leq 1/\cos(\pi/k) \cdot d(x, y)$, where $d(x, y)$ is the Euclidean distance from x to y [47].

For any given error threshold, the following lemma bounds the number of cones k.

Lemma 11: For any given positive constant ϵ ($\epsilon \to 0$), in order to guarantee $d(x, y) \leq d_k(x, y) \leq (1+\epsilon) \cdot d(x, y)$ for any pair of points $x, y \in \mathbb{R}^2$, it suffices to set $k \approx \frac{\sqrt{2}}{2}\pi\epsilon^{-1/2}$.

Proof: We use two order approximation of Taylor expansion to rewrite the result of Lemma 10 as follows

$$1/\cos(\pi/k) \cdot d(x, y) \approx 1/(1 - 1/2 * (\pi/k)^2) \cdot d(x, y) \approx (1 + 1/2 * (\pi/k)^2) \cdot d(x, y). \quad (28)$$

To guarantee that $d(x, y) \leq d_k(x, y) \leq (1 + \epsilon) \cdot d(x, y)$, we set $\epsilon = 1/2 * (\pi/k)^2$. Hence $k \approx \frac{\sqrt{2}}{2}\pi\epsilon^{-1/2}$. □

Accordingly, the objective for the weighted Fermat-Weber problem is changed to be

$$\textbf{min } F(p) = \sum_{i=1}^{n} w_j d_k(p, s_i) \quad (29)$$

for any considered point p. By Lemma 11 this yields an approximation of the original weighted sum of distance which is accurate to within a factor of ϵ.

By similar analysis in [47], we can rewrite Eq. 29 as

$$F(p) = \sum_{j=1}^{k}(\sum_{i=1}^{n} w_j ||t_j(s_i)|| \cdot [t_j(p) \leq t_j(s_i)] - ||t_j(p)|| \sum_{i=1}^{n} w_j \cdot [t_j(p) \leq t_j(s_i)]), \quad (30)$$

note that $t_j(y) \leq t_j(x)$ means point x dominates y in the coordinate system c_j (*i.e.*, $t_j(y)[1] \leq t_j(x)[1]$ and $t_j(y)[2] \leq t_j(x)[2]$), and we adopt Kenneth Iverson's notation where $[X]$ equals 1 if the predicate X is true and 0 otherwise [50].

2) Range Tree Construction: To facilitate the calculation of Eq. 30, we build 2D range trees for fast dominance queries.

The 2D range tree on a set of points is a recursively defined 2-level balanced binary search tree. Let $t_j(s'_1)[1], t_j(s'_2)[1], \ldots, t_j(s'_n)[1]$ be a sequence of the first coordinates of chargers in increasing order. A 1D range tree on $t_j(s'_1)[1], t_j(s'_2)[1], \ldots, t_j(s'_n)[1]$ is a complete binary search tree whose leaves correspond to the intervals $[t_j(s'_1)[1], t_j(s'_2)[1])$, $[t_j(s'_2)[1], t_j(s'_3)[1])$, $\ldots, [t_j(s'_{n-1})[1], t_j(s'_n)[1]]$; each internal node stores the largest value contained in its left subtree. A 2D range tree consists of a primary 1D range tree on the set $t_j(s'_1)[1], t_j(s'_2)[1], \ldots, t_j(s'_n)[1]$, and each node v of this tree contains a pointer to a secondary 1D range tree that contains all points $t_j(s_i)$ such that $t_j(s_i)[1]$ belongs to the interval of v, and builds on their second coordinate $t_j(s_i)[2]$.

Different from traditional range trees that are used to find the set of points that lie inside a given interval, or that used in [47], the purpose for our 2D range tree is to report directly the evaluations of $\sum_{i=1}^{n} w_j ||t_j(s_i)|| \cdot [t_j(p) \leq t_j(s_i)]$ and $\sum_{i=1}^{n} w_j \cdot [t_j(p) \leq t_j(s_i)]$, two crucial terms in Eq. 30. For this reason, we associate with each node in every secondary 1D range trees attached in our 2D range tree two additional parameters, which corresponds to the above two terms respectively. Note that we have to construct k number of 2D range trees for all cones to evaluate Eq. 30.

Lemma 12: Given a set S of n points in $\mathbb{R}^2$, S can be preprocessed in $O(kn \log n)$ time and space so that for any query point p, the objective function (29) can be evaluated in $O(k \log n)$ time.

3) Description of Approximation Algorithm: We show our approximation algorithm for the Fermat-Weber problem in Algorithm 2. Let P be the set of all lines that compose skew coordinate systems. As the first step, we add for each charger s_i a copy of each line in P and partition the whole area into pieces $\Gamma = \{\Gamma_1, \Gamma_2, \ldots, \Gamma_{n_\Gamma}\}$. Fig. 12(a) visualizes an instance where the whole 2D plane is divided into 57 cells given 4 chargers and $k = 6$. It follows from the definition of $F(p)$ that $F(p)$ is a convex function on $\mathbb{R}^2$ and each cell of the plane Γ_i is a linear piece. Subsequently, $F(p)$ should be minimized at a vertex of Γ, and a simple yet efficient prune-and-search algorithm is adopted to find the minimum point

Algorithm 2 Approximation Algorithm for the Fermat-Weber Problem With Maximum Distance Constraint

Input: The chargers set $S = \{s_1, s_2, \ldots, s_n\}$, the associated weights $w_1, w_2, \ldots, w_n$, error threshold ϵ.

Output: The maximum EMR point p^*.

1: Transform the 2D rectangular coordinates to k number of skew coordinates under error threshold ϵ;
2: Build k number of 2D rang trees to store skew coordinates for each charger, and provide fast evaluation for two terms in Eq. 30;
3: Employ prune-and-search algorithm to find the unconstrained Weber center $p^{*(1)}$;
4: **if** $p^{*(1)}$ locates in the constrained area $\overline{\Lambda}_j$ **then**
5: $p^* = p^{*(1)}$;
6: **else**
7: Consider the convex arc chain $\widetilde{q_1\ q_2}$ on the boundaries of $\overline{\Lambda}_j$ which is visible from the minimum point $p^{*(2)}$, apply method of Lagrange multipliers in each cell Γ_i that contains any part of the convex arc chain $\widetilde{q_1\ q_2}$ to find the local minimum point, then pick the minimum point p^* among those local minimum points.
8: **end if**

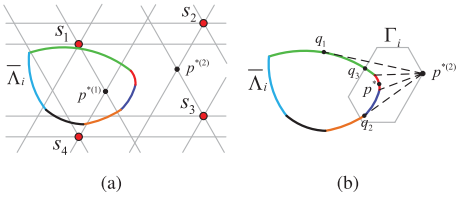

Fig. 12. Illustration of searching algorithm. (a) Plane division. (b) Search on an arc chain.

in $\mathbb{R}^2$ [47]. The corresponding time to compute such point is $O(k^2n + kn\log n)$.

As the feasible region for $F(p)$ is indeed constrained, we need to evaluate the feasibility of the obtained minimum point. In Fig. 12(a), if the minimum point, labeled as $p^{*(1)}$, lies exactly in the feasible region, say $\overline{\Lambda}_j$, then we are done. Otherwise, we need to consider the convex arc chain on the boundaries of $\overline{\Lambda}_j$ which is visible from the minimum point $p^{*(2)}$ [28]. In Fig. 12(b), the arc chain is composed by 2 consecutive arcs, namely $\widetilde{q_1\ q_3}$ and $\widetilde{q_3\ q_2}$. The number of intersection points of Γ and $\widetilde{q_1\ q_2}$ is at most $2kn$, and thus the number of arcs is at most $2kn + 1$. This is because there are kn lines on the plane and the arc chain is convex.

To find the minimum point p^* on the arc chain, we need to analyze each arc segment to find its local minimum point and then pick out the global minimum point among them. Each arc segment lies in different cells, and therefore our task finally boils down to find the minimum point on a linear 2D plane constrained by an arc segment. This problem can be addressed by method of Lagrange multipliers [51]. We omit the details here to save space.

Theorem 13: For any given small number ϵ, our algorithm to FWNC can achieve $(1-\epsilon)$ approximation ratio in deterministic $O(\epsilon^{-1}n + \epsilon^{-1/2}n^2)$ time and $O(\epsilon^{-1/2}n\log n)$ space.

Proof: Please see Appendix for the detailed proof. □

F. Theoretical Analysis

Theorem 14: For any given small number ϵ, the solution $p^{\#}$ obtained by our algorithm and the optimal solution p^* satisfy $(1-\epsilon)e(p^*) \leq e(p^{\#}) \leq e(p^*)$. The computational time complexity is $O(\epsilon^{-2}n^3 + \epsilon^{-3/2}n^4)$, and the space requirement is $O(\epsilon^{-1/2}n\log n)$, where n is the number of chargers in the input active charger set.

Proof: Please see Appendix for the detailed proof. □

VI. Simulation Results

A. Evaluation Setup

We assume that there are 12 chargers uniformly deployed over a $100\,m \times 100\,m$ 2D square area and 100 devices randomly deployed in the area too. We set $\alpha = 10^5$, $\beta = 40$ and $D = 60$ for the charging model, and $c_1 = 1$ for the EMR model. For the utility model, we simply set $c_2 = 0.001$. Moreover, the error threshold of the SCP algorithm is $\epsilon = 0.12$, and the EMR threshold is $R_t = 150$. Note that the result is averaged by 100 instances with different random seeds and device deployments.

B. Baseline Setup

In Section VI-C1, we compare the MEP algorithm to the particle swarm optimization (PSO) [52] with the number of particles set to be 20 and the loop count be 200. In addition, we use a fine-grained exhaustive search method to find the MEP on the plane, and take its output as the optimal solution.

The first is the optimal solution obtained by enumerating all possible activations of chargers in SCP. Note that here the constraints in SCP are outputs of the optimal solution for MEP used in Section VI-C1. The second is the near optimal solution. It is identical to the optimal solution except that its EMR threshold is set to be $(1-\epsilon)R_t$. The third is a greedy algorithm for SCP whose constraints are derived based on our approximation algorithm for MEP. Particularly, the greedy algorithm turns on the charger that yields the maximum overall additional utility for all devices while does not violate the EMR safety requirement at each step. Such process repeats until no further activation is possible in terms of EMR safety.

C. Performance Comparison

In this subsection, we examine the performance of our approximation algorithm for MEP in terms of approximation threshold ϵ, and that for SCP under various designs with different system parameters including the threshold ϵ, the charger number and the EMR threshold R_t.

1) Impact of MEP Threshold ϵ: To show the efficiency of our MEP algorithm, we consider 50 chargers and 100 devices uniformly deployed over a $500\,m \times 500\,m$ 2D square area, and investigate the performance of our approximation algorithm for MEP and other two baseline algorithms in terms of the MEP threshold ϵ. As illustrated in Fig. 13, the outputs of the optimal solution and the PSO are 170.2 and 161.9 respectively and remain constant. The maximal EMR computed by our algorithm decreases with an increasing ϵ. It is always greater than that of the PSO and is at most 4% smaller than that of the optimal solution for $0.12 \leq \epsilon \leq 0.3$. This indicates that the approximation bound $(1-\epsilon)$ strictly holds.

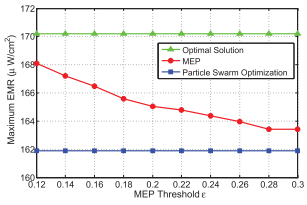

Fig. 13. Maximal EMR vs. MEP Threshold ϵ.

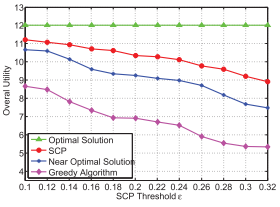

Fig. 14. Overall Utility vs. SCP Threshold ϵ.

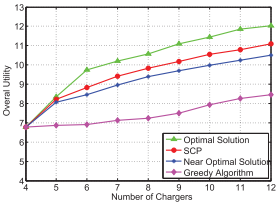

Fig. 15. Overall Utility vs. Charger Number n.

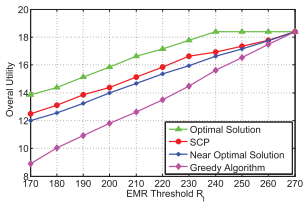

Fig. 16. Overall Utility vs. EMR Threshold R_t.

2) Impact of SCP Threshold ϵ: We proceed to examine the influence of the SCP threshold ϵ on the overall utility and plot the results in Fig. 14. As can be seen, the overall utility of the optimal solution is constant and equal to 12. Our SCP algorithm always outperforms that of the near optimal solution, and the performance gap with the optimal solution diminishes when ϵ decreases and is equal to 6.7% when $\epsilon = 0.1$. This observation is consistent with our intuition that higher error leads to low accuracy, and validates our theoretical findings. In addition, the greedy algorithm has the worst performance, which is overall roughly 34.6% below that of our SCP algorithm.

3) Impact of Charger Number n: We are also interested in the impact of the charger number on overall utility. Fig. 15 shows that all algorithms have the same performance when the charger number is 4. This is because the activation of all 4 chargers will never damage the EMR safety and thus there is no room for improvement. Besides, the overall utility of every algorithm increases smoothly with the number of chargers, and our SCP algorithm performs better than the near optimal algorithm, and the performance difference from the optimal one is at most 9.3%. The gap between the SCP algorithm and the greedy algorithm can be as large as 26.4%.

4) Impact of EMR Threshold R_t: We study the effect of the EMR threshold R_t to the overall utility in this subsection. As shown in Fig. 16, not surprisingly, the overall utility of all considered solutions grows with an increasing R_t. The performance of our SCP algorithm also outperforms the near optimal solution. Overall, the optimal solution is nearly 7.7% higher than that of our SCP algorithm, which in turn enjoys an average performance gain of 14.9% over the greedy algorithm. Furthermore, when R_t exceeds 240, the activation of all 12 chargers is allowed for the sake of EMR safety, and thereby the overall utility of the optimal solution reaches the maximum 18.4 and remains constant from then on. The same situation occurs to the other three algorithms when R_t exceeds 270.

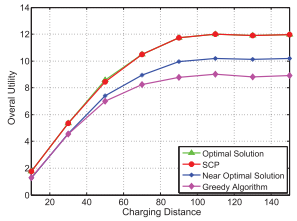

Fig. 17. Overall Utility vs. Charging Distance D.

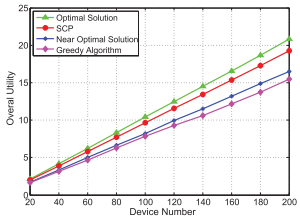

Fig. 18. Overall Utility vs. Device Number m.

5) Impact of Charging Distance D: We study the impact of charging distance D on the overall utility, and illustrate the results in Fig. 17. We can see that the utility for all the four algorithms steadily increases until D reaches $110\,m$, and from then on become relatively stable. The achieved utility for our SCP algorithm is almost the same as that of the optimal solution, and it outperforms the near optimal solution and greedy algorithm by on average 20.1% and 29.7%, respectively. Moreover, when the charging distance exceeds 110, each charger can cover most of the deployed area, and therefore, increasing D provides negligible performance gain to the overall utility and the utility keeps nearly unchanged.

6) Impact of Device Number m: Fig. 18 shows how the overall utility changes when the device number m increases from 20 to 200. Obviously, the utility for all the four algorithms are nearly proportional to the number of device number. The reason is that the devices are uniformly distributed in the considered area and every data point is obtained by averaging the results of 100 instances, therefore, the scheduling schemes given different number of devices are nearly the same, and the overall utility is thus determined by the density of devices, or the number of devices. On average, the achieved utility of SCP outperforms the near optimal and greedy algorithms by 16.5% and 24.5%, respectively, and is 7.1% inferior compared with the optimal solution.

D. Insights

In this section, we explain why our proposed scheme can obtain a high overall utility gain. We conduct a simulation and observe the utility of each of 50 devices, as shown in Fig. 19. Since the charging utility of a device is proportional to the EMR there (please refer to their definitions in Section III-A), the utility distribution of devices actually reflects the EMR

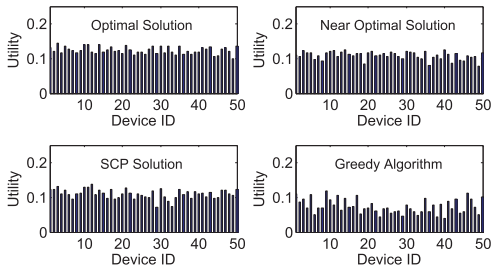

Fig. 19. Utility of devices for four solutions.

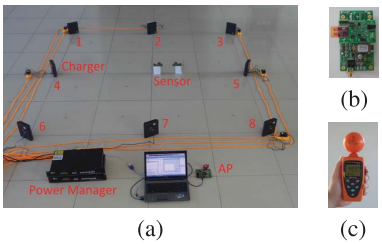

Fig. 20. Illustration of field experiment. (a) Testbed. (b) Sensor node. (c) RF field strength meter.

distribution for the locations of devices. Intuitively, if all the EMRs at the locations of devices are quite close to the EMR threshold R_t, which means that the EMRs are balanced among these locations, the overall utility will be high. From the top two sub-figures of Fig. 19, we can see that the utility of all 50 devices are nearly uniform, and close to 150 and 132 respectively, which are the theoretical maximum utility constrained by their EMR safety requirements. As for the bottom two sub-figures, the greedy algorithm has utility distribution with a higher variance. This is because the greedy algorithm is conducted in such a way that it totally overlooks the balance of EMR distribution. The EMRs at certain points on the plane shall rise much quickly than others during the greedy process of activating new chargers, and soon approach R_t and disable further charger activation. Hence, its overall achieved utility is low. Conversely, our SCP solution performs in a reasonable manner so that the utility is balanced among devices and thus is improved significantly. Note that our SCP solution is essentially a conservative algorithm in that all the constraints obtained by the MEP algorithm are actually more rigorous than that in the optimal solution, thus its maximum individual utility of devices is relatively smaller than that of the optimal solution. So does the greedy algorithm.

VII. Experimental Results

Fig. 20(a) shows the indoor experimental testbed. We utilize 8 chargers (TX91501 transmitters produced by Powercast [3]) which are deployed on the vertices and middle points of edges of a $2.4\,m * 2.4\,m$ square area. In addition, we place one wireless rechargeable sensor node (see Fig. 20(b)) at the center of the square area, and the other to the right side of the first one with distance $0.4\,m$. We use an RF field strength meter (see Fig. 20(c)) to measure the intensity of EMR. It is noteworthy that all the chargers are actually directional. With reasonable precision, we model their charging region as a sector with angle $60°$ and radius 4, whose bisector is perpendicular to the charger. Further, the fitting EMR function

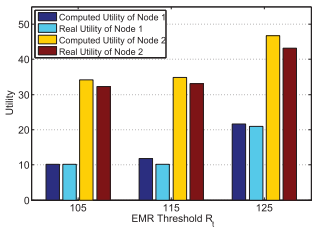

Fig. 21. Utility vs. R_t.

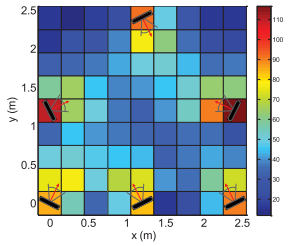

Fig. 22. An EMR distribution example.

in the sector is $\frac{41.93}{(d+0.6428)^2}$ ($D = 4$, refer to Eq. 1 if needed). The orientation of chargers should thus greatly impact the EMR distribution of the space. Suppose the chargers are numbered from top to bottom and from left to right as shown in Fig. 20(a). We rotate chargers from 1 to 8 such that the angles between their orientation and the positive horizontal line are $296.56°$, $296.56°$, $243.44°$, $26.56°$, $153.44°$, $63.44°$, $116.56°$ and $116.56°$, respectively, in order to enhance the charging efficiency in the square area. The computer controls the power supply through a power manager. The sensor nodes record their received power and send the information to an access point (AP) connecting to the computer. The AP then reports the data to the computer for analysis and decision.

We make the following adaptations to our SCP algorithm considering real situations. First, we adjust our SCP algorithm to the case under directional chargers. This can be done by modifying our MEP algorithm. We omit the details to save space. Second, to alleviate the error incurred by modeling of directional chargers, environmental variation, etc., we let the two sensors sample the charging power from each charger at the beginning of the algorithm. Then we perform our SCP algorithm based on the sampled values.

As Fig. 21 illustrates, we compare the computed utility based on sampling with real utility under three different values of R_t. Note that Node 1 refers to the node located at the center of the area and Node 2 refers to the other. We can see that the computed utility of both nodes is always larger than the real utility, but the difference between them is quite small and no more than 7.5%. This observation supports the power additivity assumption and the effectiveness of our sampling approach. Furthermore, the gap between these two solutions tends to increase when the utility grows. This is likely due to the charging property of the capacitors in sensors. Suppose the EMR threshold R_t is $125\,\mu W/cm^2$, we turn on charger 2, 4, 5, 6, 7 and 8 according to the output of our adapted algorithm. Then we measure the EMR values at $9 * 9$ grid points of the square region, and plot them in Fig. 22 to visualize the EMR distribution of the area in an approximation manner. We observe that the EMR peaks at the location of charger 5 and is equal to $116.7\,\mu W/cm^2$ and thus less than R_t. This fact confirms the correctness of our SCP algorithm.

VIII. Conclusions

In this paper, we have studied the problem of maximizing the charging utility under the constraints of EMR safety. Considering the complexity of the original problem, we broke it down into two related subproblems, *i.e.*, SCP and MEP. For MEP, we proposed a series of novel techniques to transform it into a classical problem FWNC. These techniques combined with our tailored approximation algorithm for FWNC form a $(1-\epsilon)$ solution. Based on the powerful results of MEP, we presented a near optimal solution to SCP. To evaluate the effectiveness of our solution, we conducted both extensive simulations and field experiments. All of their results corroborated our analytical findings. This solution could be incorporated into many systems to harness the detrimental impact of EMR.

There are some future promising research directions as far as I am concerned. The first direction is to explore for more precise and elegant but less computational demanding methods than the area discretization techniques adopted in this paper. The second is to consider charging tasks dynamically generated by rechargeable devices rather than one-time optimization of aggregate utility for devices to cater to the needs of real applications. The third is to adopt more realistic charging models such as directional charging models and practical energy superposition models. The fourth is to assume that chargers and/or devices have some degree of capability to move around, such as move within a disk area, and thereby consider the charging utility optimization problem.

References

[1] A. Kurs *et al.*, "Wireless power transfer via strongly coupled magnetic resonances," *Science*, vol. 317, no. 5834, pp. 83–86, 2007.

[2] *WISP*. Accessed: 2017. [Online]. Available: http://www.seattle.intel-research.net/wisp/

[3] *Powercast*. Accessed: 2017. [Online]. Available: http://www.powercastco.com

[4] *Powermat*. Accessed: 2017. [Online]. Available: http://www.powermat.com

[5] *Dell Laptop*. Accessed: 2017. [Online]. Available: http://www.laptopmag.com/reviews/laptops/dell-latitude-3330.aspx

[6] *Halo*. Accessed: 2010. [Online]. Available: http://evworld.com/news.cfm?newsid=24420

[7] *Sharp*. Accessed: 2017. [Online]. Available: http://www.friendsofcrc.ca/projects/sharp/sharp.html

[8] *Wireless Power Transmission Market Forecast*. Accessed: 2014. [Online]. Available: https://www.electronics.ca/store/wireless-power-transmission-market-forecast-analysis.html

[9] M. Buettner, R. Prasad, M. Philipose, and D. Wetherall, "Recognizing daily activities with RFID-based sensors," in *Proc. ACM UbiComp*, 2009, pp. 51–60.

[10] M. Buettner, R. Prasad, M. Philipose, and D. Wetherall, "Revisiting smart dust with RFID sensor networks," in *HotNets-VII*, 2008, pp. 1–132.

[11] C. Greene *et al.*, "Making wireless sensor networks truly wireless using RF power," IntelliSensor, Irwin, PA, USA, Tech. Rep. 1, 2010.

[12] *Data Center Environmental Monitoring*. Accessed: 2017. [Online]. Available: http://http://www.powercastsensors.com/category/applications/page/2/

[13] S. He *et al.*, "Energy provisioning in wireless rechargeable sensor networks," in *Proc. IEEE INFOCOM*, Apr. 2011, pp. 2006–2014.

[14] R. P. Wicaksono, G. K. Tran, K. Sakaguchi, and K. Araki, "Wireless grid: Enabling ubiquitous sensor networks with wireless energy supply," in *Proc. IEEE Veh. Technol. Conf. (VTC Spring)*, May 2011, pp. 1–5.

[15] *Powercast Report*. Accessed: 2014. [Online]. Available: http://http://powercastco.com/pdf/2009sensorsexpo2.pdf

[16] J. G. Shearer *et al.*, "Power transmission network," U.S. Patent 7 844 306 B2, Nov. 30, 2010.

[17] M. Olteanu *et al.*, "Dangerous temperature increase from EM radiation around metallic implants," *Acta Electrotehn.*, vol. 53, no. 2, pp. 175–180, 2012.

[18] Y. P. Shkolnikov *et al.*, "Electromagnetic interference and exposure from household wireless networks," in *Proc. PSES*, Oct. 2011, pp. 1–5.

[19] O. P. Gandhi *et al.*, "Exposure limits: The underestimation of absorbed cell phone radiation, especially in children," *Electromagn. Biol. Med.*, vol. 31, no. 1, pp. 34–51, 2011.

[20] M. Edwards *et al.*, "Effects of heat on embryos and foetuses," *Int. J. Hyperthermia*, vol. 19, no. 3, pp. 295–324, 2002.

[21] A. Karinen, S. Heinävaara, R. Nylund, and D. Leszczynski, "Mobile phone radiation might alter protein expression in human skin," *BMC Genomics*, vol. 9, no. 1, p. 77, 2008.

[22] H. Nittby *et al.*, "Exposure to radiation from global system for mobile communications at 1,800 MHz significantly changes gene expression in rat hippocampus and cortex," *Environmentalist*, vol. 28, no. 4, pp. 458–465, 2008.

[23] M. Havas *et al.*, "Provocation study using heart rate variability shows microwave radiation from 2.4 GHz cordless phone affects autonomic nervous system," *Eur. J. Oncol. Library*, vol. 5, no. 1, pp. 273–300, 2010.

[24] M. P. Ntzouni *et al.*, "Transient and cumulative memory impairments induced by GSM 1.8 GHz cell phone signal in a mouse model," *Electromagn. Biol. Med.*, vol. 32, no. 1, pp. 95–120, 2013.

[25] *Hygienic Standard for Environmental Electromagnetic Waves*. Accessed: 1987. [Online]. Available: http://www.moh.gov.cn/zwgkzt/pgw/201212/34317.shtml

[26] A. Ahlbom *et al.*, "Guidelines for limiting exposure to time-varying electric, magnetic, and electromagnetic fields (up to 300 GHz). International commission on non-ionizing radiation protection," *Health Phys*, vol. 74, no. 4, pp. 494–522, 1998.

[27] A. Fréville, "The multidimensional 0–1 knapsack problem: An overview," *Eur. J. Oper. Res.*, vol. 155, no. 1, pp. 1–21, 2004.

[28] A. P. Hurter, Jr., M. K. Schaefer, and R. E. Wendell, "Solutions of constrained location problems," *Manage. Sci.*, vol. 22, no. 1, pp. 51–56, 1975.

[29] X. Lu, P. Wang, D. Niyato, D. I. Kim, and Z. Han, "Wireless networks with RF energy harvesting: A contemporary survey," *IEEE Commun. Surveys Tuts.*, vol. 17, no. 2, pp. 757–789, 2nd Quart., 2015.

[30] X. Lu, P. Wang, D. Niyato, D. I. Kim, and Z. Han, "Wireless charging technologies: Fundamentals, standards, and network applications," *IEEE Commun. Surveys Tuts.*, vol. 18, no. 2, pp. 1413–1452, 2nd Quart., 2016.

[31] T. Soyata, L. Copeland, and W. Heinzelman, "RF energy harvesting for embedded systems: A survey of tradeoffs and methodology," *IEEE Circuits Syst. Mag.*, vol. 16, no. 1, pp. 22–57, 1st Quart., 2016.

[32] S. Zhang, Z. Qian, F. Kong, J. Wu, and S. Lu, "P^3: Joint optimization of charger placement and power allocation for wireless power transfer," in *Proc. IEEE INFOCOM*, Apr. 2015, pp. 2344–2352.

[33] I. Katsidimas, S. Nikoletseas, T. P. Raptis, and C. Raptopoulos, "Efficient algorithms for power maximization in the vector model for wireless energy transfer," in *Proc. ACM ICDCN*, 2017, Art. no. 30.

[34] H. Dai *et al.*, "Omnidirectional chargability with directional antennas," in *Proc. IEEE ICNP*, Nov. 2016, pp. 1–10.

[35] H. Dai, X. Wang, A. X. Liu, H. Ma, and G. Chen, "Optimizing wireless charger placement for directional charging," in *Proc. IEEE INFOCOM*, Jun. 2017, pp. 2922–2930.

[36] H. Dai, X. Wang, A. X. Liu, H. Ma, and G. Chen, "Safe charging for wireless power transfer," in Proc. *IEEE INFOCOM*, Apr. 2014, pp. 1105–1113.

[37] H. Dai, X. Wang, A. X. Liu, H. Ma, and G. Chen, "SCAPE: Safe charging with adjustable power," in *Proc. IEEE ICDCS*, Jun. 2014, pp. 439–448.

[38] H. Dai, X. Wang, A. X. Liu, H. Ma, and G. Chen, "Radiation constrained wireless charger placement," in *Proc. IEEE INFOCOM*, Apr. 2016, pp. 1–9.

[39] L. Li *et al.*, "Radiation constrained fair wireless charging," in *Proc. IEEE SECON*, Jun. 2017, pp. 1–9.

[40] H. Dai, H. Ma, and A. X. Liu, "Radiation constrained scheduling of wireless charging tasks," in *Proc. ACM MobiHoc*, 2017, p. 17.

[41] S. Nikoletseas, T. P. Raptis, and C. Raptopoulos, "Low radiation efficient wireless energy transfer in wireless distributed systems," in *Proc. IEEE ICDCS*, Jun. 2015, pp. 196–204.

[42] M. R. Gary and D. S. Johnson, *Computers and Intractability; A Guide to the Theory of NP-Completeness*. San Francisco, CA, USA: Freeman, 1979.

[43] W. Ge, J. Zhang, and G. Xue, "MIMO-pipe modeling and scheduling for efficient interference management in multihop MIMO networks," *IEEE Tran. Veh. Technol.*, vol. 59, no. 8, pp. 3966–3978, Oct. 2010.

[44] M. De Berg, *Computational Geometry: Algorithms and Applications*. Berlin, Germany: Springer, 2008.
[45] R. Durier and C. Michelot, "Geometrical properties of the Fermat–Weber problem," *Eur. J. Oper. Res.*, vol. 20, no. 3, pp. 332–343, 1985.
[46] S. Bespamyatnikh, K. Kedem, and M. Segal, "Optimal facility location under various distance functions," in *Algorithms and Data Structures*. Berlin, Germany: Springer, 1999, pp. 318–329.
[47] P. Bose *et al.*, "Fast approximations for sums of distances, clustering and the Fermat–Weber problem," *Comput. Geometry*, vol. 24, no. 3, pp. 135–146, 2003.
[48] C. Bajaj, "The algebraic degree of geometric optimization problems," *Discrete Comput. Geometry*, vol. 3, no. 1, pp. 177–191, 1988.
[49] R. Chandrasekaran and A. Tamir, "Algebraic optimization: The Fermat–Weber location problem," *Math. Program.*, vol. 46, nos. 1–3, pp. 219–224, 1990.
[50] D. E. Knuth, "Two notes on notation," *Amer. Math. Monthly*, vol. 99, no. 5, pp. 403–422, May 1992.
[51] I. Vapnyarskii, "Lagrange multipliers," in *Encyclopaedia of Mathematics*. Heidelberg, Germany: Springer, 2001.
[52] J. Kennedy, "Particle swarm optimization," in *Encyclopedia of Machine Learning*. Berlin, Germany: Springer, 2011, pp. 760–766.

Haipeng Dai (M'14) received the B.S. degree from the Department of Electronic Engineering, Shanghai Jiao Tong University, Shanghai, China, in 2010, and the Ph.D. degree from the Department of Computer Science and Technology, Nanjing University, Nanjing, China, in 2014. He is currently a Research Assistant Professor with the Department of Computer Science and Technology, Nanjing University. His research interests are mainly in the areas of wireless charging, mobile computing, and data mining. His research papers have been published in many prestigious conferences and journals, such as the ACM VLDB, the ACM SIGMETRICS, the ACM MobiHoc, the IEEE INFOCOM, the IEEE ICDCS, the IEEE ICNP, the ICPP, the IEEE IPSN, the IEEE TRANSACTIONS ON MOBILE COMPUTING, the IEEE TRANSACTIONS ON PARALLEL AND DISTRIBUTED SYSTEMS, and the *ACM Transactions on Sensor Networks*. He is an ACM member. He has been serving as the Poster Chair of the IEEE ICNP 2014, a TPC member of the IEEE ICNP 2014, the IEEE ICC 2014–2016, the IEEE ICCCN 2015–2016, and the IEEE Globecom 2014–2016, and ICNP 2015. He received the Best Paper Award from the IEEE.

Yunhuai Liu received the Ph.D. degree from The Hong Kong University of Science and Technology in 2008. He is currently a Professor with the Beijing Institute of Big Data Research and Peking University, Beijing, China. He has authored or coauthored over 50 publications, and his publications have appeared in the IEEE TRANSACTIONS ON PARALLEL AND DISTRIBUTED SYSTEMS, the IEEE JOURNAL ON SELECTED AREAS IN COMMUNICATIONS, the IEEE TRANSACTIONS ON MOBILE COMPUTING, and the IEEE TRANSACTIONS ON VEHICULAR TECHNOLOGY. His main research interests include wireless sensor networks, pervasive computing, and wireless network.

Guihai Chen received the B.S. degree in computer software from Nanjing University, China, in 1984, the M.E. degree in computer applications from Southeast University in 1987, and the Ph.D. degree in computer science from The University of Hong Kong in 1997. He is currently a Professor and the Deputy Chair with the Department of Computer Science, Nanjing University. He had been invited as a Visiting Professor by many foreign universities, including the Kyushu Institute of Technology, Japan, in 1998, The University of Queensland, Australia, in 2000, and Wayne State University, USA, from 2001 to 2003. He has a wide range of research interests with focus on sensor networks, peer-to-peer computing, high-performance computer architecture, and combinatorics.

Xiaobing Wu received the B.S. and M.E. degrees from Wuhan University in 2000 and 2003, respectively, and the Ph.D. degree from Nanjing University in 2009, all in computer science. He was an Associate Professor with the Department of Computer Science and Technology, Nanjing University. He is currently with the Wireless Research Centre, University of Canterbury, New Zealand. His research interests are in the fields of wireless networking and communications, Internet of Things, and cyber-physical systems. His publications appeared in the IEEE TRANSACTIONS ON PARALLEL AND DISTRIBUTED SYSTEMS, the *ACM Transactions on Sensor Networks*, *Computer Communications* (Com–Com), *Wireless Networks*, the IEEE INFOCOM 2015/2014, the IEEE ICDCS 2014, and the IEEE MASS 2013. He received the Honoured Mention Award in ACM MobiCom 2009 Demos and Exhibitions.

Tian He is currently an Associate Professor with the Department of Computer Science and Engineering, University of Minnesota, Twin Cities. He has authored and coauthored over 200 papers in premier sensor network journals and conferences with over 20,000 citations (H-Index 59). His research includes wireless sensor networks, cyber-physical systems, intelligent transportation systems, real-time embedded systems, and distributed systems. He has received a number of research awards in the area of networking, including five best paper awards. He was also a recipient of the NSF CAREER Award 2009 and the McKnight Land-Grant Professorship. He served a few program chair positions in international conferences and on many program committees, and also currently serves as an Editorial Board member for seven international journals including the *ACM Transactions on Sensor Networks.*

Alex X. Liu received the Ph.D. degree in computer science from The University of Texas at Austin in 2006. He received the IEEE and IFIP William C. Carter Award in 2004, the National Science Foundation CAREER Award in 2009, and the Michigan State University Withrow Distinguished Scholar Award in 2011. He received Best Paper Awards from ICNP-2012, SRDS-2012, and LISA-2010. His research interests focus on networking and security. He is an Associate Editor of the IEEE/ACM TRANSACTIONS ON NETWORKING, an Editor of the IEEE TRANSACTIONS ON DEPENDABLE AND SECURE COMPUTING, and an Area Editor of *Computer Communications.*

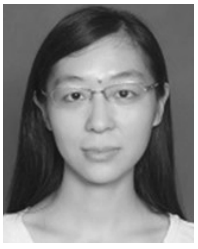

Huizhen Ma received the B.S. degree from the Department of Computer Science and Technology from Shandong University, Jinan, China, in 2015. She is currently pursuing the master's degree with the Department of Computer Science and Technology, Nanjing University. Her research interests focus on wireless charging.